Orbital tunable 0-π transitions in Josephson junctions with noncentrosymmetric topological superconductors

Yuri Fukaya,[1] Keiji Yada,[1] Yukio Tanaka,[1] Paola Gentile,[2] and Mario Cuoco[2]
[1]*Department of Applied Physics, Nagoya University, Nagoya 464-8603, Japan*
[2]*CNR-SPIN, c/o Universitá di Salerno, I-84084 Fisciano (Salerno), Italy*

(Received 12 August 2020; accepted 22 September 2020; published 13 October 2020)

We investigate the Josephson transport properties in a Josephson junction consisting of a conventional s-wave superconductor coupled to a multiorbital noncentrosymmetric superconductor marked by an orbitally driven inversion asymmetry and isotropic interorbital spin-triplet pairing. Contrary to the canonical single band noncentrosymmetric superconductor, we demonstrate that the local interorbital spin-triplet pairing is tied to the occurrence of sign-changing spin-singlet pair amplitude on different bands with d-wave symmetry. Such multiband $d^{\pm}$-wave state is a unique superconducting configuration that drives unexpected Josephson effects with 0-π transitions displaying a high degree of electronic control. Remarkably, we find that the phase state of a noncentrosymmetric/s-wave Josephson junction can be toggled between 0 and π in multiple ways through a variation of electron filling, strength of the spin-orbital coupling, amplitude of the inversion asymmetry interaction, and junction transparency. These results highlight an intrinsic orbital and electrical tunability of the Josephson response and provide unique paths to unveil the nature of unconventional multiorbital superconductivity as well as inspire innovative designs of Josephson quantum devices.

DOI: 10.1103/PhysRevB.102.144512

I. INTRODUCTION

Breaking of inversion symmetry offers an unique possibility for the design of unconventional superconducting phases [1] in noncentrosymmetric quantum materials [2,3]. In canonical single band noncentrosymmetric superconductors (NCSs), the lack of inversion symmetry naturally leads to the mixing of even (spin-singlet) and odd (spin-triplet) parity pairing configurations [4]. The resulting degree of parity mixing is a general consequence of the strong inversion asymmetric spin-orbit coupling and of the structure of the pairing interaction and can be observed in bulk materials.

In the framework of single band NCS, a lot of attention and intense research efforts have been devoted to determine the relative amplitude of the opposite parity pairing components especially for the perspective of achieving a topological superconducting phase [5–8] with the spin-triplet component being dominant. Apart from direct spectroscopic [9] or thermodynamic means to access the structure of the superconducting order parameter, a common and powerful approach is to design junctions that contain NCS interfaced to NCS or conventional s-wave superconductors (SCs). Several proposals have been put forward to assess the nature of the NCS as the formation of helical Andreev bound states (ABSs) and the corresponding anomalies in the conductance [9,10], the nonlocal features of the crossed Andreev reflections [11], the distinctive marks of the temperature dependence of the critical current [12] and the current-voltage characteristics in NCS-NCS junctions [13].

The phenomenology of the Josephson response in suitably designed heterostructure with NCS can be quite rich due to the multicomponent superconducting pairing especially when they are comparable in size. While the emergence of π states is typically bound to occur in superconductor/ferromagnet/superconductor junctions [14–16], due to the extra π shift originating from the exchange coupling in the ferromagnetic layer, the role of spin-orbit fields can bring additional channels for the generation and control of 0-π transitions. Indeed, a π-Josephson effect and 0-π transitions can be realized in NCS-NCS junctions with the two NCSs having opposite orientation of the Rashba spin-orbit field [17] or by interfacing nanowires with low-dimensional electronic channels having nontrivial geometric shape at the nanoscale [18]. An anomalous Josephson current phase relation (CPR) can be also obtained by engineering magnetic quantum dots at the NCS/s-wave spin-singlet superconductor (SSC) interface [19].

Interestingly, even without magnetic effects, when considering a junction between a conventional SSC and a NCS, one can achieve a transition between 0- and $\pi/2$-type of CPRs in the SSC/NCS junction through an anomalous ϕ-junction behavior by uniquely tuning the ratio between spin-singlet and spin-triplet component [20]. In most of these configurations it is the balance between the spin-triplet and spin-singlet components that determines the overall phase coherent response of the junction.

Differently from the case of single band NCSs, it has been recently recognized that in materials with a strong coupling between spin-orbital degrees of freedom the breaking of inversion symmetry can lead to unconventional pairing with exotic topological properties [21]. Indeed, for electronic systems with atomic spin-orbit and orbital Rashba couplings,

superconducting phases with isotropic orbital-dependent spin-triplet superconductivity can display point nodes that are topologically protected and manifest an extraordinary reconstruction of the excitation spectra both in the bulk and at the edge of the SC [21]. Compared with the conventional Rashba spin-orbit coupling [22], it has been realized that spin-momentum locking can be achieved by a pure orbitally driven asymmetric interaction. The resulting orbital Rashba effect then yields chiral orbital textures and nonstandard orbital dependent spin-textures through the atomic spin-orbit coupling [23–27]. Remarkably, apart from the complexity of the spin-orbital polarization pattern in the reciprocal space arising from the interplay of the atomic spin-orbit and orbital Rashba interactions, the spin vector of the superconducting excitations display clear hallmarks of the interorbital spin-triplet pairing with unique spin-winding around the nodal points [28]. The substantial nonstandard of the superconducting behavior for this type of multiorbital pairing configuration poses fundamental questions on the nature of the transport properties in a Josephson junction based on such NCS and in general on the role of orbital degrees of freedom in setting out the phase state of the junction.

In this paper, we demonstrate that isotropic interorbital spin-triplet pairing in NCSs generally leads to an intricate Josephson response within the electronic phase space manifesting 0-π phase transitions when considering a junction that contains a conventional spin-singlet s-wave SC. This behavior is imprinted in the emergence of a unique sign-changing intraorbital spin-singlet pair amplitude on different bands with d-wave symmetry. Due to the anisotropic and orbital-dependent sign change of the induced intraorbital spin-singlet pair amplitude in the NCS, the Josephson current manifests an intrinsic tendency to undergo a transition from a 0- to a π-phase state. We determine the phase diagram associated with the 0 and π states in the space spanned by the strength of the atomic spin-orbit coupling ($\lambda_{\rm SO}$) and the orbital Rashba interaction ($\Delta_{\rm is}$) for various electron filling factor. Due to the subtle orbital dependence of the induced intraorbital spin-singlet pair amplitude, the increase of the electron filling tends to activate more orbital channels and in turn stabilize the π-phase state in a large portion of the [$\Delta_{\rm is}$, $\lambda_{\rm SO}$] parameters space. The temperature dependence of the maximal Josephson current has an anomalous behavior for a junction orientation that is parallel to the nodal direction with a low-temperature rapid upturn that arises due to the presence of flat surface ABSs [29–32]. A variation of the orientation leads to a dominant second harmonic contribution in the Josephson current originating from the zero-energy surface ABSs. Due to the orbital tunability, the Josephson effect can bring unique fingerprints to unveil the nature of unconventional multiorbital superconductivity as well as inspire innovative designs of Josephson quantum devices.

The structure of the paper is as follows. In Sec. II, we introduce the model Hamiltonian and the methodology to determine the Josephson current. Section III is devoted to the analysis of the induced intraorbital spin-singlet pair amplitude in the bulk. Then, we present the behavior of the CPR in Sec. IV in terms of the spin-orbital interactions by varying the electron filling and discuss the origin of the sign change in the Josephson current. Section V is devoted to the study of the temperature dependence of the maximum Josephson current. Finally, the discussion and the concluding remarks are presented in Sec. VI.

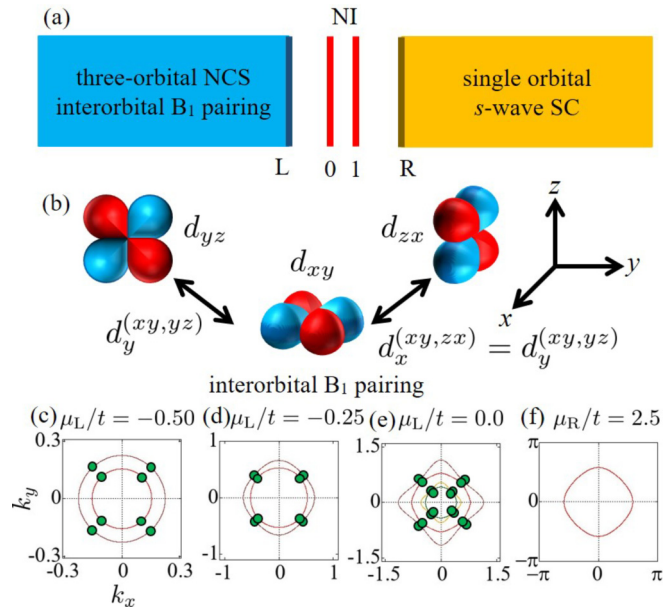

FIG. 1. (a) Sketch of the noncentrosymmetric superconductor (NCS)/normal (NI)/single orbital s-wave superconductor (SC). In the NCS, the interorbital B_1 pairing belongs to the C_{4v} point group [21]. (b) Schematic illustration of interorbital spin-triplet pairing with B_1 symmetry in the three-orbital NCS which is based on the mixing of the d_{xy} with d_{zx} and d_{yz} orbitals [21]. [(c)–(e)] Fermi surface of NCS for $\lambda_{\rm SO}/t = 0.10$ and $\Delta_{\rm is}/t = 0.20$. We choose three representative chemical potentials as (c) $\mu_L/t = -0.50$, (d) -0.25, and (e) 0.0. Filled circles denote the position of the nodes for the interorbital B_1 pairing. (f) Fermi surface of the single orbital s-wave SC at the chemical potential $\mu_R/t = 2.5$.

II. MODEL AND METHODOLOGY

In this section, we introduce the model Hamiltonian and the methodology that has been employed to calculate the Josephson current for the three-orbital NCS/single band s-wave SC junction.

A. Model Hamiltonian

In the superconducting state we adopt a Bogoliubov-de Gennes (BdG) description. The left-side SC [Fig. 1(a)] of the junction refers to a three-orbital NCS with isotropic interorbital spin-triplet pairing as schematically indicated in Fig. 1(b). For this type of SC, the BdG Hamiltonian can be generally expressed in the following form:

$$\hat{H}^{\rm L}_{\rm BdG}(\boldsymbol{k}) = \begin{pmatrix} \hat{H}_{\rm L}(\boldsymbol{k}) & \hat{\Delta}_{\rm L} \\ \hat{\Delta}^{\dagger}_{\rm L} & -\hat{H}^{*}_{\rm L}(-\boldsymbol{k}) \end{pmatrix}. \tag{1}$$

The Hamiltonian for the normal state $\hat{H}_{\rm L}(\boldsymbol{k})$ describes the electronic states of d orbitals belonging to the t_{2g} manifold and is given by

$$\hat{H}_{\rm L}(\boldsymbol{k}) = \hat{H}_0(\boldsymbol{k}) + \hat{H}_{\rm SO} + \hat{H}_{\rm is}(\boldsymbol{k}), \tag{2}$$

with the three terms $\hat{H}_0(\boldsymbol{k})$, $\hat{H}_{\rm SO}$, and $\hat{H}_{\rm is}(\boldsymbol{k})$ [21,33] being associated with the orbital dependent kinetic energy, the atomic spin-orbit coupling, and the orbital Rashba interaction, respectively. The first term denotes the kinetic part,

$$\hat{H}_0(\boldsymbol{k}) = \hat{\varepsilon}(\boldsymbol{k}) \otimes \hat{\sigma}_0, \tag{3}$$

where $\hat{\sigma}_{i=x,y,z,0}$ are the Pauli matrices and the identity matrix in the spin space. $\hat{\varepsilon}(\boldsymbol{k})$ corresponds to the intraorbital kinetic energy for each t_{2g} orbital,

$$\hat{\varepsilon}(\boldsymbol{k}) = \begin{pmatrix} \varepsilon_{yz}(\boldsymbol{k}) & 0 & 0 \\ 0 & \varepsilon_{zx}(\boldsymbol{k}) & 0 \\ 0 & 0 & \varepsilon_{xy}(\boldsymbol{k}) \end{pmatrix}, \tag{4}$$

$$\varepsilon_{yz}(\boldsymbol{k}) = -\mu_{\rm L} + 2t_3(1-\cos k_x) + 2t_1(1-\cos k_y), \tag{5}$$

$$\varepsilon_{zx}(\boldsymbol{k}) = -\mu_{\rm L} + 2t_1(1-\cos k_x) + 2t_3(1-\cos k_y), \tag{6}$$

$$\varepsilon_{xy}(\boldsymbol{k}) = -\mu_{\rm L} + 4t_2 - 2t_2\cos k_x - 2t_2\cos k_y + \Delta_{\rm t}, \tag{7}$$

with $\mu_{\rm L}$ being the chemical potential of the NCS. $\hat{H}_{\rm SO}$ expresses the canonical atomic spin-orbit coupling and is given by

$$\hat{H}_{\rm SO} = \lambda_{\rm SO}[\hat{l}_x \otimes \hat{\sigma}_x + \hat{l}_y \otimes \hat{\sigma}_y + \hat{l}_z \otimes \hat{\sigma}_z], \tag{8}$$

where $\lambda_{\rm SO}$ is the amplitude of the atomic spin-orbit interaction, $\hat{l}_{j=x,y,z}$ are the orbital angular momentum operators in the basis (d_{yz}, d_{zx}, d_{xy}) projected out of the $L = 2$ space. They are expressed as

$$\hat{l}_x = \begin{pmatrix} 0 & 0 & 0 \\ 0 & 0 & i \\ 0 & -i & 0 \end{pmatrix}, \quad \hat{l}_y = \begin{pmatrix} 0 & 0 & -i \\ 0 & 0 & 0 \\ i & 0 & 0 \end{pmatrix},$$
$$\hat{l}_z = \begin{pmatrix} 0 & i & 0 \\ -i & 0 & 0 \\ 0 & 0 & 0 \end{pmatrix}. \tag{9}$$

The third term in $\hat{H}_{\rm L}$ stands for the antisymmetric orbital Rashba interaction and is given by

$$\hat{H}_{\rm is}(\boldsymbol{k}) = \Delta_{\rm is}[\hat{l}_y \sin k_x - \hat{l}_x \sin k_y] \otimes \hat{\sigma}_0, \tag{10}$$

with $\Delta_{\rm is}$ being the strength of the inversion symmetry breaking coupling. In the examined three-orbital NCS, we consider a form of interorbital local pairing that has been extensively studied in Refs. [21,28]. There, the pair potential $\hat{\Delta}_{\rm L}$ can be made up by components with spin-singlet/orbital-triplet/s-wave and spin-triplet/orbital-singlet/s-wave pairing symmetry. Thus the pair potential $\hat{\Delta}_{\rm L}$ is described by the t_{2g}-orbital characters $\alpha, \beta = yz, zx, xy$ for each interorbital pairing symmetry,

$$\hat{\Delta}_{\rm L}^{(\alpha,\beta)} = i\hat{\sigma}_y\psi^{(\alpha,\beta)} + i[\boldsymbol{d}^{(\alpha,\beta)} \cdot \hat{\boldsymbol{\sigma}}]\hat{\sigma}_y, \tag{11}$$

where $\psi^{(\alpha,\beta)}$ is the spin-singlet/orbital-triplet pair potential and $\boldsymbol{d}^{(\alpha,\beta)}$ are the **d** vectors,

$$\boldsymbol{d}^{(xy,yz)} = \left(d_x^{(xy,yz)}, d_y^{(xy,yz)}, d_z^{(xy,yz)}\right),$$
$$\boldsymbol{d}^{(xy,zx)} = \left(d_x^{(xy,zx)}, d_y^{(xy,zx)}, d_z^{(xy,zx)}\right),$$
$$\boldsymbol{d}^{(yz,zx)} = \left(d_x^{(yz,zx)}, d_y^{(yz,zx)}, d_z^{(yz,zx)}\right).$$

The spin-triplet/orbital-singlet state for each interorbital isotropic pairing is described by the following **d** vectors,

$$\hat{\Delta}_{\rm L}^{(\alpha,\beta)} = \begin{pmatrix} \Delta_{\uparrow\uparrow}^{(\alpha,\beta)} & \Delta_{\uparrow\downarrow}^{(\alpha,\beta)} \\ \Delta_{\downarrow\uparrow}^{(\alpha,\beta)} & \Delta_{\downarrow\downarrow}^{(\alpha,\beta)} \end{pmatrix}$$
$$= \begin{pmatrix} -d_x^{(\alpha,\beta)} + id_y^{(\alpha,\beta)} & d_z^{(\alpha,\beta)} \\ d_z^{(\alpha,\beta)} & d_x^{(\alpha,\beta)} + id_y^{(\alpha,\beta)} \end{pmatrix}.$$

In this study, we consider an interorbital pairing state belonging to the B_1 representation of the C_{4v} point group [Fig. 1(b)] that is the most favorable energetically among all the allowed interorbital pairings [21]. This pairing state is described by a pure spin-triplet configuration and exhibits nodal points along the diagonal direction [Figs. 1(c)–1(e)] which are topologically protected by the chiral symmetry of the BdG Hamiltonian [21]. The **d** vector of the interorbital B_1 pairing state is given by

$$d_x^{(xy,zx)} = d_y^{(xy,yz)},$$
$$\Delta_{xy,yz}^{\uparrow\uparrow} = \Delta_{xy,yz}^{\downarrow\downarrow} = id_y^{(xy,yz)},$$
$$\Delta_{xy,zx}^{\uparrow\uparrow} = -\Delta_{xy,zx}^{\downarrow\downarrow} = -d_x^{(xy,zx)}. \tag{12}$$

We point out that a different **d**-vector orientation is associated with the interorbital pairing when mixing the (d_{xy}, d_{zx}) or (d_{xy}, d_{yz}) orbitals.

On the other hand, for the description of the right-side SC in the junction we consider a canonical single orbital s-wave state,

$$\hat{H}_{\rm BdG}^{\rm R}(\boldsymbol{k}) = \begin{pmatrix} \hat{H}_{\rm R}(\boldsymbol{k}) & \hat{\Delta}_{\rm R} \\ \hat{\Delta}_{\rm R}^{\dagger} & -\hat{H}_{\rm R}^{*}(-\boldsymbol{k}) \end{pmatrix}. \tag{13}$$

Here, $\hat{H}_{\rm R}(\boldsymbol{k})$ denotes the Hamiltonian in the normal state for the single orbital model,

$$\hat{H}_{\rm R}(\boldsymbol{k}) = \xi_{\rm R}(\boldsymbol{k}) \otimes \hat{\sigma}_0, \tag{14}$$

$$\xi_{\rm R}(\boldsymbol{k}) = -\mu_{\rm R} + 4t_4 - 2t_4\cos k_x - 2t_4\cos k_y, \tag{15}$$

with $\mu_{\rm R}$ being the chemical potential of the single orbital s-wave SC. The pair potential $\hat{\Delta}_{\rm R}$ is given by

$$\hat{\Delta}_{\rm R} = i\hat{\sigma}_y\psi_{\rm R}, \tag{16}$$

with the spin-singlet/s-wave pair potential $\psi_{\rm R}$.

In the normal layers between the two SCs, we consider the following single orbital model Hamiltonian:

$$\hat{H}_{\rm NI}(\boldsymbol{k}) = \xi_{\rm NI}(\boldsymbol{k}) \otimes \hat{\sigma}_0, \tag{17}$$

$$\xi_{\rm NI}(\boldsymbol{k}) = -\mu_{\rm NI} + 4t_5 - 2t_5\cos k_x - 2t_5\cos k_y, \tag{18}$$

with $\mu_{\rm NI}$ being the chemical potential setting the electron density at the normal insulating layer.

In our calculation, we set the parameters as $t_2 = t_1 = t_4 = t_5 = t$, $t_3 = 0.10t$, $\Delta_{\rm t} = -0.50t$, $\mu_{\rm R} = 2.5t$, and $\mu_{\rm NI} = -0.50t$. In addition, we fix the critical temperature of the two SCs as $T_{\rm cL}/t = 1.0 \times 10^{-5}$ and $T_{\rm cR}/t = 10T_{\rm cL}$. Then, we assume that the gap amplitude of the SCs $\Delta_{\rm L}(T)$ and $\Delta_{\rm R}(T)$ has a BCS-like temperature

dependence T,

$$\Delta_X(T) = \Delta_X(0)\tanh\left[1.74\sqrt{\frac{T_{cX}-T}{T}}\right],$$
$$\Delta_X(0) = \frac{3.53}{2}T_{cX}, \tag{19}$$

where $X = \mathrm{L}, \mathrm{R}$ denotes the index for the left and right-side SCs within the junction, respectively.

B. Recursive Green's function approach

In order to compute the Josephson current, we employ the recursive Green's function method [34]. As shown in Fig. 1(a), we consider the two semi-infinite SCs and two normal layers sandwiched between the SCs as studied in Ref. [35]. Firstly, we calculate the semi-infinite surface Green's functions for the left and right-side SCs $G_{\mathrm{L}}(k_\parallel, i\varepsilon_n)$ and $G_{\mathrm{R}}(k_\parallel, i\varepsilon_n, \phi)$ with $i\varepsilon_n = i(2n+1)\pi k_{\mathrm{B}}T$ being the fermionic Matsubara frequency, ϕ the phase difference between two SCs, and $k_\parallel$ the momentum that is parallel to the interface. When we include the normal layers at the boundary of a SC, these surface Green's functions, i.e., $G_{\mathrm{L0}}(k_\parallel, i\varepsilon_n)$ and $G_{\mathrm{R1}}(k_\parallel, i\varepsilon_n, \phi)$, are given by

$$G_{\mathrm{L0}}(k_\parallel, i\varepsilon_n) = [i\varepsilon_n - \hat{u}_{\mathrm{NI}} - \hat{t}^\dagger_{\mathrm{L,NI}}G_{\mathrm{L}}(k_\parallel, i\varepsilon_n)\hat{t}_{\mathrm{L,NI}}]^{-1}, \tag{20}$$

$$G_{\mathrm{R1}}(k_\parallel, i\varepsilon_n, \phi) = [i\varepsilon_n - \hat{u}_{\mathrm{NI}} - \hat{t}_{\mathrm{R,NI}}G_{\mathrm{R}}(k_\parallel, i\varepsilon_n, \phi)\hat{t}^\dagger_{\mathrm{R,NI}}]^{-1}, \tag{21}$$

with $\hat{u}_{\mathrm{NI}}$ setting the on-site electron density of the normal layer. Here, $\hat{t}_{\mathrm{L,NI}}$ ($\hat{t}_{\mathrm{R,NI}}$) means the tunnel Hamiltonian between left- (right)-side SC and the normal insulating layer,

$$\hat{t}_{\mathrm{X,NI}}(k_\parallel) = \begin{pmatrix} \tilde{t}_{\mathrm{X,NI}}(k_\parallel) & 0 \\ 0 & -\tilde{t}^*_{\mathrm{X,NI}}(-k_\parallel) \end{pmatrix}. \tag{22}$$

In the (100) direction, these are described by

$$\tilde{t}_{\mathrm{L,NI}}(k_\parallel) = t_{\mathrm{int}}\begin{pmatrix} -t & 0 \\ -t & 0 \\ -t & 0 \\ 0 & -t \\ 0 & -t \\ 0 & -t \end{pmatrix}, \tag{23}$$

$$\tilde{t}_{\mathrm{R,NI}}(k_\parallel) = t_{\mathrm{int}}\begin{pmatrix} -t & 0 \\ 0 & -t \end{pmatrix}, \tag{24}$$

and in the (110) direction,

$$\tilde{t}_{\mathrm{L,NI}}(k_\parallel) = t_{\mathrm{int}}\begin{pmatrix} t(k_\parallel) & 0 \\ t(k_\parallel) & 0 \\ t(k_\parallel) & 0 \\ 0 & t(k_\parallel) \\ 0 & t(k_\parallel) \\ 0 & t(k_\parallel) \end{pmatrix}, \tag{25}$$

$$\tilde{t}_{\mathrm{R,NI}}(k_\parallel) = t_{\mathrm{int}}\begin{pmatrix} t(k_\parallel) & 0 \\ 0 & t(k_\parallel) \end{pmatrix}, \tag{26}$$

with $t(k_\parallel) = -2t\cos k_\parallel$ and t_{int} setting the degree of the junction's transparency. Next, when connecting two SCs with a normal layer as shown in Fig. 1(a), one can calculate the local Green's functions $G_{00}(k_\parallel, i\varepsilon_n, \phi)$ and $G_{11}(k_\parallel, i\varepsilon_n, \phi)$,

$$G_{00}(k_\parallel, i\varepsilon_n, \phi) = \left[G^{-1}_{\mathrm{L0}}(k_\parallel, i\varepsilon_n) - \hat{t}_{\mathrm{NI}}G_{\mathrm{R1}}(k_\parallel, i\varepsilon_n, \phi)\hat{t}^\dagger_{\mathrm{NI}}\right]^{-1}, \tag{27}$$

$$G_{11}(k_\parallel, i\varepsilon_n, \phi) = \left[G^{-1}_{\mathrm{R1}}(k_\parallel, i\varepsilon_n, \phi) - \hat{t}^\dagger_{\mathrm{NI}}G_{\mathrm{L0}}(k_\parallel, i\varepsilon_n)\hat{t}_{\mathrm{NI}}\right]^{-1}, \tag{28}$$

and the nonlocal Green's functions $G_{01}(k_\parallel, i\varepsilon_n, \phi)$ and $G_{10}(k_\parallel, i\varepsilon_n, \phi)$,

$$G_{01}(k_\parallel, i\varepsilon_n, \phi) = G_{\mathrm{L0}}(k_\parallel, i\varepsilon_n, \phi)\hat{t}_{\mathrm{NI}}(k_\parallel)G_{11}(k_\parallel, i\varepsilon_n, \phi), \tag{29}$$

$$G_{10}(k_\parallel, i\varepsilon_n, \phi) = G_{\mathrm{R1}}(k_\parallel, i\varepsilon_n, \phi)\hat{t}^\dagger_{\mathrm{NI}}(k_\parallel)G_{00}(k_\parallel, i\varepsilon_n, \phi), \tag{30}$$

with the $\hat{t}_{\mathrm{NI}}(k_\parallel)$ being the nearest-neighbor hopping term in the normal layer. Concerning the current operator, one can calculate the Josephson current $I_{\mathrm{c}}(\phi)$ at a given phase difference ϕ between the left and right side of the junction by evaluating the following expression:

$$I_{\mathrm{c}}(\phi) = \frac{ie}{\hbar}\int_{-\pi}^{\pi}\mathrm{Tr}' k_{\mathrm{B}}T\sum_{i\varepsilon_n}[\hat{t}_{\mathrm{NI}}(k_\parallel)G_{01}(k_\parallel, i\varepsilon_n, \phi) - \hat{t}^\dagger_{\mathrm{NI}}(k_\parallel)G_{10}(k_\parallel, i\varepsilon_n, \phi)]dk_\parallel. \tag{31}$$

Here, Tr' means the trace over the electronic degrees of freedom. In this study, we focus on three representative types of spin-resolved Fermi surfaces for the NCS at $\mu_{\mathrm{L}}/t = -0.50$ [Fig. 1(c)], $\mu_{\mathrm{L}}/t = -0.25$ [Fig. 1(d)], and $\mu_{\mathrm{L}}/t = 0.0$ [Fig. 1(e)], and we fix the chemical potential of the single orbital s-wave SC at $\mu_{\mathrm{R}}/t = 2.5$ [Fig. 1(f)]. In the NCS, we consider the spin-split Fermi surfaces with both nonzero spin-orbit coupling λ_{SO} and the orbital Rashba interaction Δ_{is}. At $\mu_{\mathrm{L}}/t = -0.50$ [Fig. 1(c)] and $\mu_{\mathrm{L}}/t = -0.25$ [Fig. 1(d)], there are two Fermi surfaces and the d_{xy} is the dominant orbital component at the Fermi level. On the other hand, for $\mu_{\mathrm{L}}/t = 0.0$ [Fig. 1(e)], the number of Fermi surfaces is four and these Fermi surfaces typically include all t_{2g} orbitals. We can thus evaluate the influence of the orbital character and the number of Fermi surfaces by calculating the Josephson current for each selected μ_{L}.

III. INDUCED INTRAORBITAL SPIN-SINGLET PAIR AMPLITUDE

We start by analyzing the induced intraorbital spin-singlet pair amplitude for the three representative types of spin-split Fermi surfaces as shown in Figs. 1(c)–1(e) at $\mu_{\mathrm{L}}/t = -0.50$, $\mu_{\mathrm{L}}/t = -0.25$, $\mu_{\mathrm{L}}/t = 0.0$ and we will consider its profile both in the bulk and in the following section at the junction's interface.

In the Josephson junction upon examination, the even-frequency spin-singlet pairing components in both left and right-side SCs can interfere and contribute to the first harmonic term of the overall Josephson current. For this reason, it is useful to investigate the spin-singlet components of the pair amplitude on the Fermi surfaces in the NCS both in the inner side at a given k in the reciprocal space or along the edge of the junction's interface for the conserved component of the momentum. Hereafter, we indicate as $F^{(\alpha,\beta)}_{\uparrow\downarrow-\downarrow\uparrow}(k)$ the spin-

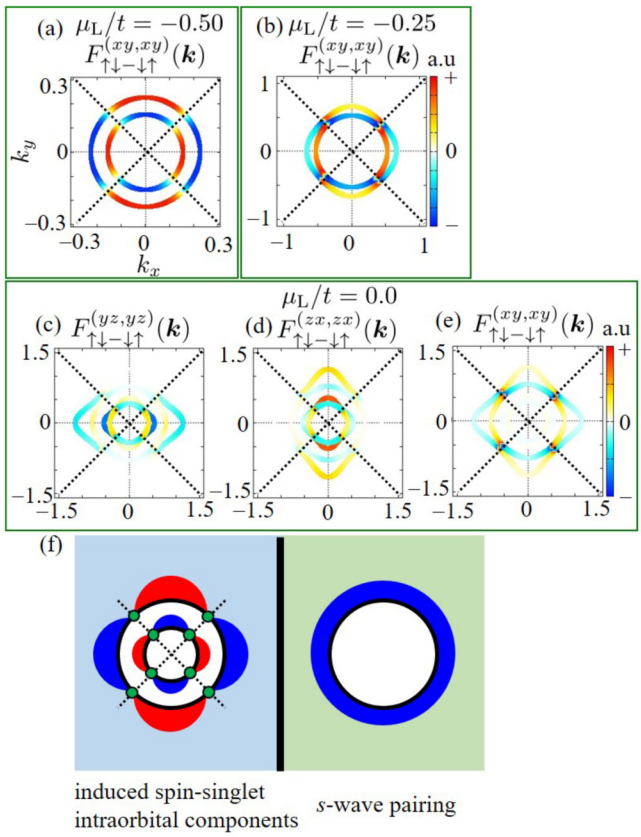

FIG. 2. Even-frequency spin-singlet intraorbital pairing amplitude on the Fermi surfaces with d_{xy} character evaluated in the bulk of the NCS at (a) $\mu_L/t = -0.50$ and (b) -0.25. Spin-singlet intraorbital pairing amplitude with (c) d_{yz}, (d) d_{zx}, and d_{xy} orbital character in the NCS bulk at $\mu_L/t = 0.0$. All even-frequency spin-singlet intraorbital components have the $d^{\pm}_{x^2-y^2}$-wave structure with sign change when comparing with the inner and outer Fermi surfaces. (f)Schematic illustration of the Josephson junction. Black dotted line denotes the direction along which nodal points occur while green circles stand for the position of the node. We set the parameters as $\lambda_{SO}/t = 0.10$, $\Delta_{is}/t = 0.20$ for the spin-orbit and orbital Rashba couplings and the temperature is $T = 0.10T_{cL}$.

singlet pair amplitude associated with the electron pairing in the orbitals (α, β) at a given value of the momentum k.

Regarding the bulk NCS, we find that at the Fermi surface, for the two representative values of the chemical potential $\mu_L/t = -0.50$ and -0.25, the intraorbital spin-singlet component associated with the d_{xy} configuration has a sign-changing $d_{x^2-y^2}$-wave structure with nodal points along the diagonal direction for each Fermi surface as shown in Figs. 2(a) and 2(b). In particular, we point out that the sign of the pair amplitude on the inner Fermi surface is opposite as compared with that on the outer Fermi surface. Thus the intraorbital spin-singlet pair amplitude realizes a $d^{\pm}_{x^2-y^2}$-wave pairing configuration with a band dependent sign of the pair amplitude that resembles the isotropic $s_{\pm}$-wave proposed in the framework of the iron based SCs [36–38]. Likewise, at the Fermi level $\mu_L/t = 0.0$, the intraorbital spin-singlet component has also $d^{\pm}_{x^2-y^2}$-wave structure with nodal points along the diagonal direction as explicitly demonstrated in Figs. 2(c)–2(e). However, due to the contribution of the d_{zx} and d_{yz} bands, the momentum distribution of the pair amplitude is more anisotropic than the d_{xy} case when considering the corresponding intraorbital configurations [Figs. 2(d) and 2(e)]. We note that also for this $d^{\pm}_{x^2-y^2}$-wave state, the intraorbital spin-singlet component pair amplitude has opposite signs on the inner and outer Fermi surface [Figs. 2(c)–2(e)]. Thus the induced $d^{\pm}_{x^2-y^2}$-wave pairing, as schematically shown in Fig. 2(f), emerges as a relevant element to interpret and evaluate the Josephson effect especially when considering the junction with the NCS interfaced to a s-wave spin-singlet SC. Indeed, even if the interorbital spin-triplet pairing symmetry is dominant in the NCS, we expect that the induced intraorbital spin-singlet $d^{\pm}_{x^2-y^2}$-wave configuration will play a key role in setting the Josephson current and would naturally lead to a sign frustration in the Josephson current due to the sign effects at the Fermi surface. Moreover, due to the significant orbital dependence and the momentum anisotropy we also expect that 0-π transitions can be sensitive to the junction transparency.

IV. CURRENT PHASE RELATION: PHASE DIAGRAM, ROLE OF INTERFACE ORIENTATION, TRANSPARENCY, AND TEMPERATURE

In this section, we present the CPR for the interorbital B_1 state NCS/NI/single orbital s-wave SC junction (NCS/NI/SSC). The CPR can be generally expanded in Fourier series in terms of all the harmonics with respect to the applied phase difference ϕ as follows:

$$I_c(\phi) = \sum_n [I_n \sin(n\phi) + J_n \cos(n\phi)]. \tag{32}$$

Since for the examined junction both SCs have the time-reversal symmetry, the cosine term J_n equals to zero [39].

Let us first discuss the outcome of the CPR for the (100) junction orientation. In Fig. 3(a), we report the CPR assuming that the charge transfer electronic processes at the interface set out a regime of high transparency with the hopping amplitude $t_{int} = 1.0$. Hence, in order to assess the role of the orbital degree of freedom we investigate three representative chemical potentials for the NCS, i.e., $\mu_L/t = -0.50$ (red line), $\mu_L/t = -0.25$ (blue line), and $\mu_L/t = 0.0$ (green line) in Fig. 3(a). Here, when the Fermi surface is dominated only by the $d_{xy}-$orbital, we find that the CPR has a conventional sinusoidal 0-junction behavior at $\mu_L/t = -0.50$ (red line) as shown in Fig. 3(a). However, with the increase of the electron filling via μ_L, the Josephson current relation changes to a π-phase profile with a sign change [Fig. 3(a)]. This trend indicates that a 0 junction can be turned into a π junction by suitably tuning the band occupation through the chemical potential μ_L. On the other hand, for the case of low transparency ($t_{int} = 0.10$), we find that the Josephson current is always conventional and no sign change is observed [Fig. 3(b)].

A change in the junction orientation leads to a dramatic impact on the Josephson response. Indeed, if we select a junction interface with (110) direction the presence of nodal points both in the dominant isotropic interorbital spin-triplet pairing component and in the induced spin-singlet $d^{\pm}_{x^2-y^2}$-wave pairing offers the opportunity to explore a highly

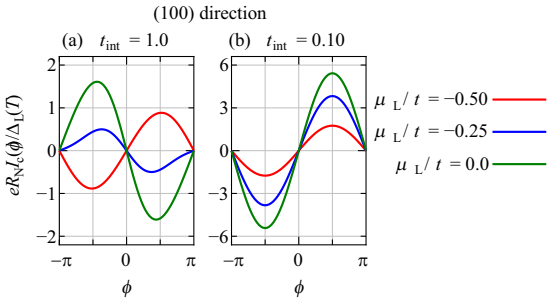

FIG. 3. Current phase relation (CPR) for the NCS/NI/SSC junction with the interface perpendicular to the (100) direction assuming that $\mu_L/t=-0.50$ (red line), -0.25 (blue line), and 0.0 (green line). The amplitude of the spin-orbital and orbital Rashba interactions corresponds to $\lambda_{SO}/t=0.10$ and $\Delta_{is}/t=0.20$. The temperature is set at $T=0.10T_{cL}$. The results correspond to two different regimes of junction's transparency: High transparency with $t_{int}=1.0$ in (a), and low transparency for $t_{int}=0.10$ in (b). We find that in the regime of high transparency there is a 0-π transition which is obtained by varying the electron filling from low to high density. For the low transparent regime at the interface (i.e., $t_{int}=0.10$), there is no phase change. This indirectly indicates that by modifying the transparency one can drive a 0-π transition.

nontrivial case of unconventional superconductivity. As for the (100) orientation, for the first harmonic term the even-frequency/spin-singlet intraorbital component in the NCS can be coupled to the even-frequency/spin-singlet pairing in the s-wave SC. However, for this case, first harmonic term I_1 vanishes since the B_1 pairing in the NCS is odd under the mirror symmetry along the diagonal direction, while SSC is even. It is the same as the case of the single band d-wave based superconducting junctions [29–32]. Moreover, the Josephson current is substantially independent of the amplitude of the chemical potential μ_L as demonstrated in Fig. 4.

Next, we study the first harmonic (I_1) contribution to the Josephson current in the (100) direction as a function of the spin-orbit coupling λ_{SO} and orbital Rashba interaction Δ_{is} in

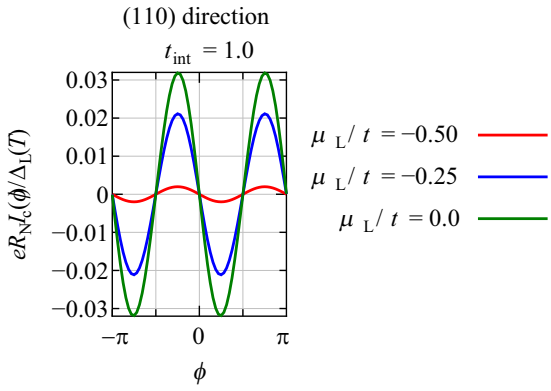

FIG. 4. CPR for the NCS/NI/SSC junction in the (110) direction for $\mu_L/t=-0.50$ (red line), -0.25 (blue line), and 0.0 (green line). We set the amplitude of the spin and orbital electronic parameters as $\lambda_{SO}/t=0.10$, $\Delta_{is}/t=0.20$, $t_{int}=1.0$, and $T=0.10T_{cL}$. In the (110) the second harmonic contribution dominates the Josephson current behavior.

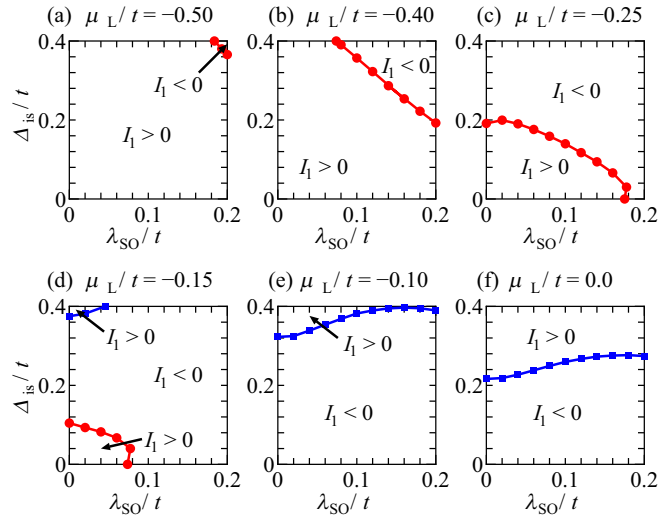

FIG. 5. Phase diagram reporting the 0 and π phases, which are determined by evaluating the sign of the first harmonic term of the Josephson current I_1 for the NCS/NI/SSC of the (100) direction in the parameters space spanned by the spin-orbit coupling (λ_{SO}/t) and the inversion symmetry breaking term (Δ_{is}/t). We consider the impact of the electron filling variation by determining the phase diagram for various values of the NCS chemical potential: (a) $\mu_L/t=-0.50$, (b) -0.40, (c) -0.25, (d) -0.15, (e) -0.10, and (f) 0.0. The other parameters are set at $t_{int}=1.0$ and $T=0.99T_{cL}$.

the regime of high transparency since we have seen that only in that case one can observe a 0-π phase transition. Apart from the role of the electron filling of the various bands, it is important to assess whether a variation of the electronic parameters associated with the strength of the spin-orbital entanglement and of the inversion asymmetry breaking can be employed to drive the 0- to π-phase transition. The outcome is remarkable and unveils an intricate interplay between the band occupation (i.e., the orbital character of the Fermi surfaces) and the combination of λ_{SO} and Δ_{is}. In Fig. 5, we present the resulting phase diagram constructed by evaluating the sign of the first harmonic term I_1 in the Josephson current in each point of the parameters space. We notice that there can be one or two boundaries that separate the 0 ($I_1>0$) from the π-phase ($I_1<0$) region in the parameters space (λ_{SO}, Δ_{is}). This implies that a reentrant type of 0-π transition can be also obtained. For instance, by increasing the orbital Rashba coupling at $\mu_L=-0.15$ for values of the λ_{SO} lower than about $0.10t$, one can achieve a 0-π-0 changeover of the Josephson CPR. Another trend that can be deduced by inspection of the phase diagram is that the increase of the chemical potential μ_L moves or generates 0-π phase boundaries. The 0-π boundary (red line in Fig. 5) shrinks towards the point $(\lambda_{SO}, \Delta_{is})=(0,0)$ by increasing the chemical potential. On the other hand, at higher values of the electron filling, another boundary (blue line in Fig. 5) occurs at a lower threshold of the orbital Rashba coupling Δ_{is}. This phenomenon can be mainly ascribed to the t_{2g}-orbital components and the anisotropy of the spin-split Fermi surfaces with both nonzero λ_{SO} and Δ_{is}. It is particularly relevant to observe that in the low electron density regime, with only two Fermi surfaces and dominant d_{xy} character, the π phase can be

achieved only for enough large λ_{SO} and Δ_{is}. Indeed, π phase at $\mu_L/t = -0.50$ appears at large (λ_{SO}, Δ_{is}) [Fig. 5(a)]. The increase of the electron filling favors the interorbital mixing and the spin-orbital coupling can in turn activate the π-phase with smaller thresholds in the amplitude. When going through the Lifshitz transition [40] from two to four Fermi surface electronic configuration, one observes an optimal regime for the π phase that now covers almost the whole phase space in the explored λ_{SO} and Δ_{is} amplitude. This outcome unveils the subtle role of the orbital degree of freedom in setting the π state in the Josephson junction. Additionally, having found a 0-π transition both in terms of a change in the electron filling and of the orbital Rashba coupling, we argue that this type of Josephson junction can manifest a dramatic response to an application of a gate voltage. We note that the behavior in Fig. 5 holds in the low temperatures since 0-π transition does not occur by changing the temperature.

In order to get more insight into the origin of the sign change of the Josephson current in the (100) direction in terms of the variation of the chemical potential μ_L in the regime of high transparency $t_{int} = 1.0$, we check the relation between the first harmonic term of the Josephson current I_1 in the (100) direction and the induced intraorbital spin-singlet pair amplitude at the interface as a function of the conserved momentum k_y (Fig. 6). The pair amplitude $\hat{F}_X$ is obtained by evaluating

$$\tilde{G}_X = \frac{1}{i\varepsilon_n - \hat{H}^X_{BdG}} = \begin{pmatrix} \hat{G}_X & \hat{F}_X \\ \bar{F}_X & \bar{G}_X \end{pmatrix}. \quad (33)$$

In the case of the three-orbital NCS (left-side SC), the pair amplitude for the (α, β) orbitals $\hat{F}^{(\alpha,\beta)}_L$ is described by

$$\hat{F}^{(\alpha,\beta)}_L = \begin{pmatrix} F^{(\alpha,\beta)}_{\uparrow\uparrow} & F^{(\alpha,\beta)}_{\uparrow\downarrow-\downarrow\uparrow} + F^{(\alpha,\beta)}_{\uparrow\downarrow+\downarrow\uparrow} \\ -F^{(\alpha,\beta)}_{\uparrow\downarrow-\downarrow\uparrow} + F^{(\alpha,\beta)}_{\uparrow\downarrow+\downarrow\uparrow} & F^{(\alpha,\beta)}_{\downarrow\downarrow} \end{pmatrix}, \quad (34)$$

and the single orbital s-wave SC $\hat{F}_R$,

$$\hat{F}_R = \begin{pmatrix} F_{\uparrow\uparrow} & F_{\uparrow\downarrow-\downarrow\uparrow} + F_{\uparrow\downarrow+\downarrow\uparrow} \\ -F_{\uparrow\downarrow-\downarrow\uparrow} + F_{\uparrow\downarrow+\downarrow\uparrow} & F_{\downarrow\downarrow} \end{pmatrix}. \quad (35)$$

In the Josephson junction upon examination, the spin-singlet pairing components in both left and right-side SCs can interfere and contribute to the first harmonic term I_1 of the overall Josephson current. For this reason, it is useful to focus on the spin-singlet pair components and in particular to have a close inspection of their behavior at the junction's interface by computing the k-resolved amplitude. Here, $F^{(\alpha,\beta)}_{\uparrow\downarrow-\downarrow\uparrow}(k_y)$ refers to the NCS while $F_{\uparrow\downarrow-\downarrow\uparrow}(k_y)$ is for the spin-singlet amplitude in the single band s-wave SC.

As expected, the spin-singlet pair amplitude in the NCS is nonvanishing due to the combination of atomic spin-orbit coupling λ_{SO} and orbital Rashba interaction Δ_{is}. Since the intraorbital components are larger than the interorbital ones regarding the B_1 representation, the behavior of the intraorbital terms is more relevant for evaluating their role in setting out the Josephson current. The analysis has been conducted with the aim to identify the driving mechanisms or key

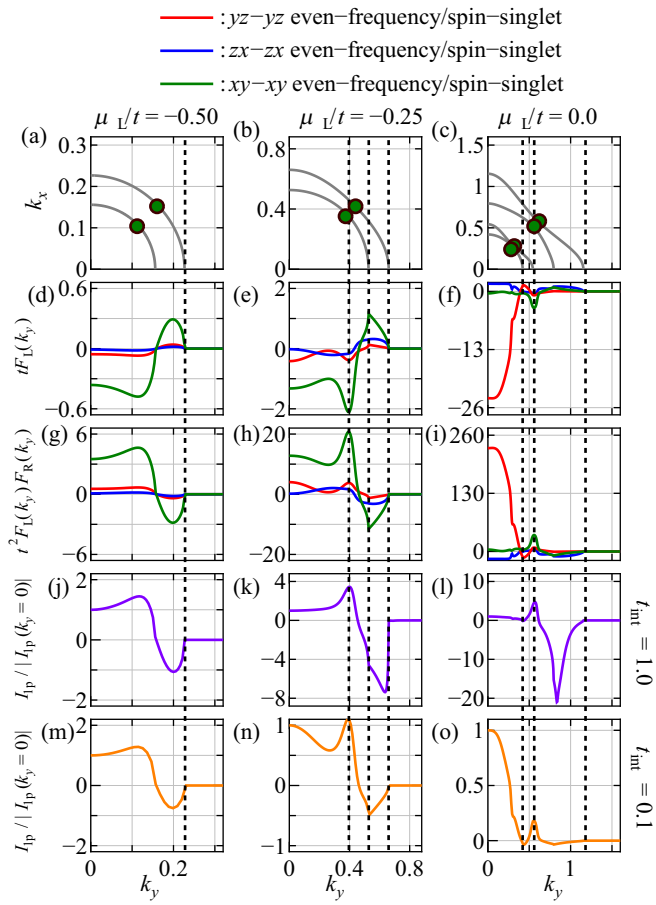

FIG. 6. Fermi surface in the NCS at (a) $\mu_L/t = -0.50$, (b) -0.25, and (c) 0.0. Pair amplitude of intraorbital spin-singlet component for each t_{2g} orbital in the NCS $F_L(k_y) = F^{(\alpha,\alpha)}_{\uparrow\downarrow-\downarrow\uparrow}$ ($\alpha = yz, zx, xy$) at (d) $\mu_L/t = -0.50$, (e) -0.25, and (f) 0.0. Product of F_L with F_R where $F_R(k_y) = F_{\uparrow\downarrow-\downarrow\uparrow}$ is the spin-singlet pairing amplitude in the single orbital s-wave SC at (g) $\mu_L/t = -0.50$, (h) -0.25, and (i) 0.0, respectively. We note that F_L and F_R are calculated in the semi-infinite systems. Momentum resolved first harmonic term $I_{1p}(k_y)$ of the Josephson current normalized by $I_{1p}(k_y = 0)$ for high trasparency ($t_{int} = 1.0$) in (j)–(l) and low transparency ($t_{int} = 0.10$) in (m)–(o), respectively. In these panels, we select the chemical potential of the NCS as $\mu_L/t = -0.50$ for (j) and (m), $\mu_L/t = -0.25$ for (k) and (n), and $\mu_L/t = 0.0$ for (l) and (o). Here, we obtain the first harmonic term $I_{1p}(k_y)$ by the summation over the Matsubara frequency at $i\varepsilon_n = -i\pi k_B T$ and $i\pi k_B T$. The other parameters are $\lambda_{SO}/t = 0.10$, $\Delta_{is}/t = 0.20$, and $T = 0.10T_{cL}$.

physical quantities behind the formation of the π state in the junction. As we have seen in the previous section, the intraorbital spin-singlet pair amplitude in the bulk has a sign change on the inner and outer Fermi surfaces with d-wave pattern. Then the CPRs which come from the outer and inner Fermi surfaces in the bulk NCS compete each other. This kind of cancellation has been proposed in iron-based $s_\pm$ SC/canonical SSC Josephson junction [41]. Moreover, a closer inspection of the amplitude distribution in the momentum space reveals a sublte anisotropy. Indeed, for the lowest electron filling ($\mu_L/t = -0.50$) the strength of the spin-singlet pairing is larger along the k_x or k_y symmetry directions, while in the intermediate electron density, corresponding to $\mu_L/t = -0.25$,

the pair amplitude is more enhanced close to the diagonal directions. A similar behavior is also obtained for the d_{xy} projected spin-singlet pairing at $\mu_L/t = 0.0$. For this electron filling, the d_{zx} or d_{yz} components, on the other hand, have a significant amplitude difference along the outer Fermi surfaces indicating that for those momenta the sign change cannot result into a complete cancellation when contributing to the Josephson processes. Specific aspects that point to sign competition and anisotropy are also found for the k_y-projected intraorbital spin-singlet pair amplitude at the edge of the NCS close to the junction interface. We generally find that the intraorbital spin-singlet pair amplitude F_L tends to have a sign change for momenta k_y [Figs. 6(d)–6(f)] that are in between those associated with the nodal points of the spin-triplet gap in the NCS [Figs. 6(a)–6(c)]. Moreover, F_L can have a high intensity for values of k_y corresponding to the Fermi wave vectors at $k_y = 0$ or nearby the nodal points. Those momenta are characteristic of the nodal topological SCs and of the underlying Fermi surface. In particular, it is useful to highlight the k_y distribution of the intraorbital spin-singlet F_L amplitude. The outcome of the analysis indicates a strong orbital and electron filling dependence. The d_{xy} component has comparable amplitude at small and large k_y for $\mu_L/t = -0.50$ and -0.25, respectively, while for a higher electron filling (e.g., $\mu_L/t = 0.0$) the dominant spectral weight is distributed at large value of k_y towards the position of the nodal points. On the other hand, the behavior of the d_{zx} and d_{yz} pairing amplitude is quite different from that of the d_{xy}. Indeed, the spectral distribution of the d_{zx} indicates that the corresponding spin-singlet pairing amplitude is mostly contributing when k_y is close to the nodal points momenta. Hence, the behavior of the induced spin-singlet pair amplitude at the edge typically changes sign as a function of k_y and its amplitude is strongly dependent on the orbital character and electron filling.

With this know-how, we are ready to evaluate a possible link between the behavior of the k-resolved intraorbital spin-singlet pair amplitude with that of the first harmonic term of the Josephson current. In particular, in the tunneling regime the product of the left and right intraorbital spin-singlet component $F_L F_R$ can be directly compared with the first harmonic Josephson term I_1. Indeed, for such configuration we have that $I_1 \sim F_L F_R$ as one can deduce by comparing the results in Figs. 6(g), 6(h), and 6(i) with those in Figs. 6(m), 6(n), and 6(o). The lack of a π-phase state emerges out of a subtle competition between the positive and negative Josephson channels when inspecting the k-resolved first harmonic term. Here, $I_{1p}(k_y)$ is obtained by the summation over the Matsubara frequency at $i\varepsilon_n = -i\pi k_B T$ and $i\pi k_B T$,

$$I_1 \propto \sum_{k_y} I_{1p}(k_y), \quad I_{1p}(k_y) \sim I_{1p}(k_y, -i\pi k_B T) + I_{1p}(k_y, i\pi k_B T).$$

On the contrary, for high transparency, the behavior of $I_{1p}(k_y)$ does not correlate with that of the intraorbital spin-singlet pairing amplitude product in Figs. 6(g), 6(h), and 6(i). Since the conductance at the high transparency is larger than that at the low transparency for large momentum as shown in Fig. 7, $I_{1p}(k_y)$ can be more affected by the contribution of multiple injection and reflection processes for the various momenta. We find that the contributions of the large momentum regions to the Josephson current are those that allow to turn the sign from positive to negative when integrating the Josephson current over all of the momenta k_y.

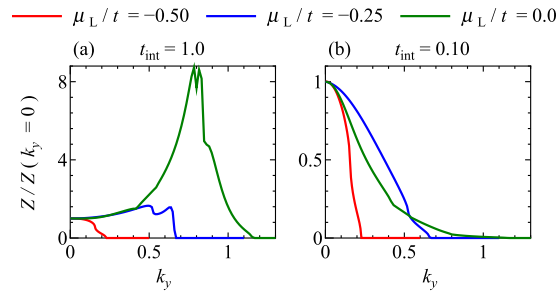

FIG. 7. Normalized charge conductance with normal metal configurations in the two sides of the junction at (a) $t_{int} = 1.0$ and (b) 0.10. Red, blue, and green lines denote the examined chemical potentials, i.e., $\mu_L/t = -0.50$, -0.25, and 0.0, respectively. We set the parameters as $\lambda_{SO}/t = 0.10$ and $\Delta_{is}/t = 0.20$.

V. TEMPERATURE DEPENDENCE OF JOSEPHSON CURRENT

In this section, we present the temperature dependence of the maximum Josephson current. The behavior of the maximum Josephson current for the temperature T depends on the zero-energy surface ABSs at the interface's junction [29–32]. In the present case, since the s-wave SC does not have the surface ABSs at the edge, we focus on the surface ABSs in the NCS. For the (100) direction, the helical edge states appear in the case with two Fermi surfaces and the surface ABSs not connecting at the zero-energy appear in the case with four Fermi surfaces [21]. In the (110) direction, zero-energy flat bands occur due to the topological properties of the nodal points in the NCS [21].

For these zero-energy surface ABSs, we can expect that the maximum Josephson current increases as the temperature is reduced [29–32]. Figure 8(a) shows the temperature depen-

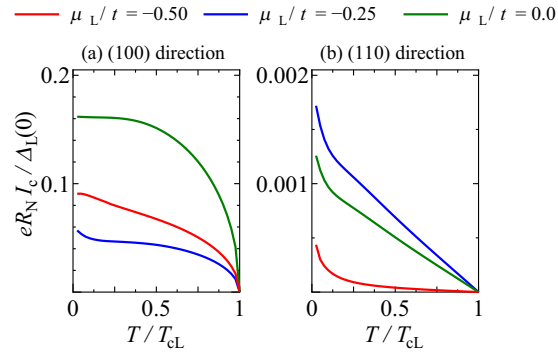

FIG. 8. Temperature dependence of the maximum Josephson current regarding the interorbital B_1 state in the NCS for the NCS/NI/SC junction. (a) Temperature dependence of the maximum Josephson current in (100) junction at $\mu_L/t = -0.50$ (red line), -0.25 (blue line), and 0.0 (green line). (b)Temperature dependence of the maximum Josephson current in (110) junction at $\mu_L/t = -0.50$ (red line), -0.25 (blue line), and 0.0 (green line). The parameters are $\lambda_{SO}/t = 0.10$, $\Delta_{is}/t = 0.20$, and $t_{int} = 1.0$.

dence of the maximum Josephson current at $\mu_L/t = -0.50$ (red line), -0.25 (blue line), and 0.0 (green line) in the (100) direction. At $\mu_L/t = -0.50$ and -0.25, the Josephson current tends to increase, however, at $\mu_L/t = 0.0$ its amplitude saturates at low temperature. As we have shown in the previous section, intraorbital even-frequency/spin-singlet/$d^{\pm}_{x^2-y^2}$-wave pair amplitude can be coupled to spin-singlet s-wave state thus directly affecting the Josephson current. The emergent properties of the intraorbital even-frequency/spin-singlet/$d^{\pm}_{x^2-y^2}$-wave components [Fig. 5(f)] can also determine the behavior of the temperature dependence of the maximum Josephson current. In the (100) direction, since the sign of the intraorbital even-frequency/spin-singlet/$d^{\pm}_{x^2-y^2}$-wave pair amplitude does not change at the interface, the thermal behavior of the Josephson current is not influenced by the spin-singlet pair amplitude. As a result, the Josephson current increases at low temperature due to the zero-energy surface ABSs at $\mu_L/t = -0.50$ and -0.25, and is saturated by no zero-energy surface ABSs at $\mu_L/t = 0.0$ [12].

Likewise, we determine the temperature dependence of maximum Josephson current in the (110) direction as shown in Fig. 8(b) at $\mu_L/t = -0.50$ (red line), -0.25 (blue line), and 0.0 (green line). At low temperature, the Josephson current shows a rapid upturn owing to the zero-energy surface ABSs. These zero-energy surface ABSs indicate that the sign of the intraorbital even-frequency/spin-singlet/$d^{\pm}_{x^2-y^2}$-wave pair amplitude changes for processes associated with the (110) direction. Thus the Josephson current in the (110) direction increases at very low temperature due to the anisotropy of the intraorbital even-frequency/spin-singlet/$d^{\pm}_{x^2-y^2}$-wave pair amplitude of the interorbital B_1 pairing [29–32].

VI. CONCLUSIONS AND DISCUSSION

We study a Josephson junction made of an NCS with local interorbital spin-triplet pairing interfaced with a conventional spin-singlet s-wave SC by considering different junction's orientation and exloring the various regimes of electron filling and spin-orbital coupling. We demonstrate that this type of superconducting pairing leads to a sign-changing intraorbital spin-singlet pair amplitude on different bands with d-wave symmetry. Such multiband $d^{\pm}$-wave state is responsible of unexpected Josephson effects with 0-π transitions displaying a high degree of electronic control. Remarkably, we find that the phase state of a NCS/NI/SSC Josephson junction can be switched between 0 and π in multiple ways through a variation of electron filling, strength of the spin-orbital coupling, amplitude of the inversion asymmetry interaction, junction orientation, and transparency. These results highlight an intrinsic orbital and electrical tunability of the Josephson response especially when considering the variation of the orbital Rashba coupling due to an applied electric field.

The presented results can find application in quantum materials where the electronic structure is marked by a strong interplay of spin and orbital degrees of freedom. This is commonly encountered in transition metal oxides and in particular at oxide interfaces or surfaces. A paradigmatic example is provided by the two-dimensional electron gas forming at the LAO-STO interface [42,43]. There, the transport properties of a suitably designed Josephson junction reveal the presence of competing 0 and π channels [44]. We argue that the interorbital pairing here studied can account, at least qualitatively, for the observed anomalies and the Josephson phase frustration as a consequence of the nontrivial surface ABSs arising from both the spin-triplet and spin-singlet pairing components.

Finally, we have proposed the spin-orbitronics functionalities to control the 0-π transitions in Josephson devices. In particular, the remarkable tunability of the Josephson effect by means of electron filling, orbital Rashba interaction and the interface's transparency indicate several ways towards an electrical design of Josephson devices by directly gating the SC or by gating the interface.

ACKNOWLEDGMENTS

This work was supported by the JSPS Core-to-Core program "Oxide Superspin" international network, and a JSPS KAKENHI (Grants No. JP15H05851, No. JP15H05853, No. JP15K21717, No. JP18H01176, No. JP18K03538, No. JP20H00131, and No. JP20H01857), and the project Quantox of QuantERA-NET Cofund in Quantum Technologies, implemented within the EU-H2020 Programme. Y.F. is supported by a JSPS research fellowship and JSPS KAKENHI (Grant No. 19J11865). M.C. and P.G. acknowledge support by the project "Two-dimensional Oxides Platform for SPIN-orbitronics nanotechnology (TOPSPIN)" funded by the MIUR Progetti di Ricerca di Rilevante Interesse Nazionale (PRIN) Bando 2017 - Grant No. 20177SL7HC.

[1] M. Sigrist and K. Ueda, Rev. Mod. Phys. **63**, 239 (1991).
[2] E. Bauer and M. Sigrist, *Lecture Notes in Physics* (Springer, Berlin, 2012), Vol. 847.
[3] M. Smidman, M. B. Salamon, H. Q. Yuan, and D. F. Agterberg, Rep. Prog. Phys. **80**, 036501 (2017).
[4] L. P. Gorkov and E. I. Rashba, Phys. Rev. Lett. **87**, 037004 (2001).
[5] Y. Tanaka, Y. Mizuno, T. Yokoyama, K. Yada, and M. Sato, Phys. Rev. Lett. **105**, 097002 (2010).
[6] K. Yada, M. Sato, Y. Tanaka, and T. Yokoyama, Phys. Rev. B **83**, 064505 (2011).
[7] M. Sato, Y. Tanaka, K. Yada, and T. Yokoyama, Phys. Rev. B **83**, 224511 (2011).
[8] P. M. R. Brydon, A. P. Schnyder, and C. Timm, Phys. Rev. B **84**, 020501(R) (2011).
[9] C. Iniotakis, N. Hayashi, Y. Sawa, T. Yokoyama, U. May, Y. Tanaka, and M. Sigrist, Phys. Rev. B **76**, 012501 (2007).
[10] A. B. Vorontsov, I. Vekhter, and M. Eschrig, Phys. Rev. Lett. **101**, 127003 (2008).
[11] S. Fujimoto, Phys. Rev. B **79**, 220506(R) (2009).
[12] Y. Asano and S. Yamano, Phys. Rev. B **84**, 064526 (2011).
[13] K. Borkje and A. Sudbo, Phys. Rev. B **74**, 054506 (2006).

[14] A. A. Golubov, M. Y. Kupriyanov, and E. Ilfichev, Rev. Mod. Phys. **76**, 411 (2004).
[15] A. I. Buzdin, Rev. Mod. Phys. **77**, 935 (2005).
[16] F. S. Bergeret, A. F. Volkov, and K. B. Efetov, Rev. Mod. Phys. **77**, 1321 (2005).
[17] J.-F. Liu, H. Zhang, and J. Wang, Chin. Phys. B **25**, 097503 (2016).
[18] G. Francica, M. Cuoco, and P. Gentile, Phys. Rev. B **101**, 094504 (2020).
[19] B. Sothmann and R. P. Tiwari, Phys. Rev. B **92**, 014504 (2015).
[20] L. Klam, A. Epp, W. Chen, M. Sigrist, and D. Manske, Phys. Rev. B **89**, 174505 (2014).
[21] Y. Fukaya, S. Tamura, K. Yada, Y. Tanaka, P. Gentile, and M. Cuoco, Phys. Rev. B **97**, 174522 (2018).
[22] E. I. Rashba, Sov. Phys. Solid State **2**, 1109 (1960).
[23] S. R. Park, C. H. Kim, J. Yu, J. H. Han, and C. Kim, Phys. Rev. Lett. **107**, 156803 (2011).
[24] J.-H. Park, C. H. Kim, H.-W. Lee, and J. H. Han, Phys. Rev. B **87**, 041301(R) (2013).
[25] P. Kim, K. T. Kang, G. Go, and J. H. Han, Phys. Rev. B **90**, 205423 (2014).
[26] J. Hong, J.-W. Rhim, C. Kim, S. R. Park, and J.-H. Shim, Sci. Rep. **5**, 13488 (2015).
[27] B. Kim, C. H. Kim, P. Kim, W. Jung, Y. Kim, Y. Koh, M. Arita, K. Shimada, H. Namatame, M. Taniguchi, J. Yu, and C. Kim, Phys. Rev. B **85**, 195402 (2012).
[28] Y. Fukaya, S. Tamura, K. Yada, Y. Tanaka, P. Gentile, and M. Cuoco, Phys. Rev. B **100**, 104524 (2019).
[29] Y. Tanaka and S. Kashiwaya, Phys. Rev. B **53**, R11957(R) (1996).
[30] Y. S. Barash, H. Burkhardt, and D. Rainer, Phys. Rev. Lett. **77**, 4070 (1996).
[31] Y. Tanaka and S. Kashiwaya, Phys. Rev. B **56**, 892 (1997).
[32] S. Kashiwaya and Y. Tanaka, Rep. Prog. Phys. **63**, 1641 (2000).
[33] G. Khalsa, B. Lee, and A. H. MacDonald, Phys. Rev. B **88**, 041302(R) (2013).
[34] A. Umerski, Phys. Rev. B **55**, 5266 (1997).
[35] K. Kawai, K. Yada, Y. Tanaka, Y. Asano, A. A. Golubov, and S. Kashiwaya, Phys. Rev. B **95**, 174518 (2017).
[36] I. I. Mazin, D. J. Singh, M. D. Johannes, and M. H. Du, Phys. Rev. Lett. **101**, 057003 (2008).
[37] K. Kuroki, S. Onari, R. Arita, H. Usui, Y. Tanaka, H. Kontani, and H. Aoki, Phys. Rev. Lett. **101**, 087004 (2008).
[38] Y. Bang and G. R. Stewart, J. Phys.: Condens. Matter **29**, 123003 (2017).
[39] Y. Asano, Y. Tanaka, M. Sigrist, and S. Kashiwaya, Phys. Rev. B **67**, 184505 (2003).
[40] I. M. Lifshitz, Sov. Phys. JETP **11**, 1130 (1960).
[41] A. V. Burmistrova, I. A. Devyatov, A. A. Golubov, K. Yada, Y. Tanaka, M. Tortello, R. S. Gonnelli, V. A. Stepanov, X. Ding, H.-H. Wen, and L. H. Greene, Phys. Rev. B **91**, 214501 (2015).
[42] A. Ohtomo and H. Y. Hwang, Nature (London) **427**, 423 (2004).
[43] N. Reyren, S. Thiel, A. D. Caviglia, L. F. Kourkoutis, G. Hammerl, C. Richter, C. W. Schneider, T. Kopp, A.-S. Ruetschi, D. Jaccard, M. Gabay, D. A. Muller, J.-M. Triscone, J. Mannhart, F. L. Kourkoutis, and G. Hammerl, Science **317**, 1196 (2007).
[44] D. Stornaiuolo, D. Massarotti, R. Di Capua, P. Lucignano, G. P. Pepe, M. Salluzzo, and F. Tafuri, Phys. Rev. B **95**, 140502(R) (2017).